The meaning of graylevels in backscattered electron images of bone

J. G. Skedros, R. D. Bloebaum,* K. N. Bachus, and T. M. Boyce
Bone and Joint Research Laboratories, VA Medical Center (151F), 500 Foothill Blvd., Salt Lake City, Utah 84148

Backscattered electron (BSE) imaging is considered to be a useful technique for determining relative differences in bone tissue density. However, it is not clear how graylevel variations seen in BSE images of bone tissue, which are primarily dependent on the tissue's average atomic number, correlate to tissue density (g/cm^3) and mineral content. Simulated bone tissues, ranging from 32–50% mineral by volume, were made by mixing synthetic hydroxyapatite with a simulated organic matrix. This technique allowed mineral content to be varied while mineral composition and crystallography remained constant. The densities of the simulated tissues were determined using Archimedes' principle. Average atomic numbers of the simulated tissues were interpolated from a regression of BSE graylevel against average atomic numbers of pure standard materials. A strong positive correlation was found to exist between mineral content and density ($r^2 = 0.978$) as well as between mineral content and atomic number ($r^2 = 0.965$). The average graylevel in the BSE image also exhibited a positive correlation to mineral content ($r^2 = 0.965$) and density ($r^2 = 0.923$). Graylevel variations in BSE images of simulated bone tissue were shown to be strongly correlated to density and mineral content, but only as a coincidence of their association with atomic number.

INTRODUCTION

Biomaterials and bone researchers are currently interested in the use of backscattered electron (BSE) imaging in the scanning electron microscope (SEM) for determining microscopic differences in the mineral content of bone tissue. However, the biophysical basis for graylevel variations in BSE images of bone tissue has not been experimentally demonstrated. Consequently, the meaning of graylevels in BSE images of bone is not clearly understood and its interpretation has been subject to confusion. For example, graylevel differences in BSE images of bone have been interpreted as being directly correlated to relative differences in "atomic number contrast,"[1,2] "mineral density,"[1,3–5] "mineral content,"[3,4] "mineralization levels,"[6] "density,"[2,4,5,7–10] and "mass density"[11] of the imaged bone tissue. The terms used in these studies are not necessarily synonymous and can lead to confusion and potential errors when interpreting the meaning of graylevels in BSE images of bone tissue. In fact, it has been experimentally demonstrated that the use of terms which include the word "density" conflict with the basic principles of the backscattered electron interactions and BSE imaging technology.[12] It is well documented that BSE detector output, hence image graylevel, is dependent on the energy of the incident electron beam and the average (apparent) atomic number of the specimen, provided that conventional grinding and polishing techniques are used to eliminate topographic and crystallographic contrast.[12–14] Before BSE imaging can become an effective tool for quantitative analysis of relative differences in bone mineral content, current ambiguities and controversies must be clarified and resolved.[12,15]

To avoid ambiguity inherent in current terminology, we intend to demonstrate that the term "mineral content" is appropriate nomenclature for interpreting the graylevels in BSE images of bone tissue. For the purposes of this study, the definition of mineral content is based on Richelle's conceptual model of bone mineralization[16–18] and is expressed according to the following equation:

$$\text{Mineral Content } [\%] = \frac{V_m}{V_m + V_{om}} \times 100 \quad (1)$$

where V_m is the volume of the mineral component, V_{om} is the volume of the hydrated organic matrix of

*To whom correspondence should be addressed.

CCC 0021-9304/93/010047-10

bone tissue, and the sum of these volumes is the total volume of bone tissue.[19]

Simulated bone tissues of varying mineral contents were made to test the hypothesis that graylevel changes in BSE images of these tissues are dependent mostly on changes in average atomic number, which are primarily a function of changes in mineral content.

MATERIALS AND METHODS

Minerals

Two pure minerals were used in this study: hydroxyapatite (HA), $Ca_{10}(PO_4)_6(OH)_2$ (Norian Corp., Mountain View, CA) and brushite, $CaHPO_4 \cdot 2H_2O$ (Sigma Chemical Corp., St. Louis, MO). X-ray diffraction and Fourier-transformed infrared (FTIR) spectroscopy (Norian Corp., Mountain View, CA) analyses verified that these materials were over 98% pure. To produce fine powders with crystal aggregates of similar size, small amounts of each mineral were ground for 10 min in an automated grinder. As described below, the ground brushite was used to show how mineral composition changes might influence graylevel changes in BSE images.

Two solid pellets, one of HA and one of brushite, were made using the powdered minerals and a Carver Press (Fred S. Carver, Inc., Menomonee Falls, WI) set at 10,000 psi (68.95 MPa). These two pellets were used for making comparisons between the graylevels of the pure HA and pure brushite.

Simulated organic matrix

Epoxy (QM-60 recipe, Loctite Corp., Cleveland, OH) was used to imitate the organic matrix in the simulated tissues in accordance with a previous study by Lees and Davidson.[20] Before making the simulated tissues, it was necessary to measure the density of epoxy. This was accomplished by weighing equal proportions of the catalyst and resin components in a small container of known weight and volume. The container and epoxy were then suspended by a fine wire from the hook of an analytical beam balance (Mettler H51, Mettler Instrument Co., Hightstown, NJ) and weighed while submerged in distilled water at room temperature (20°C). The volume of epoxy was determined by taking the difference between submerged weight and weight in air according to Archimedes' principle.[21] The weights of the catalyst and resin components were measured prior to mixing to avoid the artifact of trapped air bubbles during submergence. The epoxy exhibits minimal shrinkage (< 3.0%) and no stoichiometric change during curing (Personal Communication, Gary Bush, Research Division, Loctite Corp., Cleveland, OH).

Simulated bone tissues

To simulate a range of mineralization found in actual human bone tissue,[22] HA was mixed in varying volume proportions with epoxy (Table I). Simulated bone tissues with heterogeneous mineral compositions were also made by mixing HA with brushite and epoxy, allowing mineral composition to be altered while mineral content remained constant (Table I). These HA/brushite/epoxy mixtures simulated compositional changes that have been postulated to occur in actual bone tissue.[23–25]

The amount by weight of mineral and epoxy needed to make each simulated tissue was determined by multiplying the density of each of these components (Table I) by its volume fraction in the simulated tissues. The amount of mineral required for each mixture was measured to the nearest 0.0001 g (< 0.5% error). The mineral(s) and epoxy were then combined in a clean plastic weighing boat and were manually mixed with a small spatula for 20–30 min to obtain uniform mixtures with random crystallographic orientations. Using the spatula, the simulated bone tissues were compressed into 3.18-mm diameter by 3-mm-deep holes drilled into a plastic block, which will be referred to hereafter as the "specimen." The remaining amounts of each simulated bone tissue were rolled into small spheres that were approximately 7 mm in diameter and the densities were determined by Archimedes' principle. The uniformity of each mixture was confirmed by visual examination while scanning in the BSE mode at ×100 prior to capturing any image at ×200. Air bubbles trapped during mixing, which appear black in the BSE images in this study, were estimated during analysis to be less than 5% in any of the simulated bone tissues.

Specimen assembly

The following materials were inserted into drill holes in the center of the specimen and were used to calibrate the operating environment of the SEM (Table II): 98% pure magnesium oxide (MgO), 99% pure gamma aluminum oxide (Al_2O_3), 99.8% pure, 1.59-mm-diameter magnesium wire and 99.999% pure, 1.0-mm-diameter aluminum wire (Johnson Matthey/Aesar, Seabrook, NH). One magnesium wire was also inserted into a hole drilled between each pair of simulated tissues, and magnesium wires were also inserted around the periphery of the simulated tissues (Fig. 1). Graylevels of these wires were compared to each other and to a magnesium wire that was placed centrally in the specimen. These comparisons served to determine the variation in graylevel that could be attributed to nonuniformities in the thickness of the gold coating. The centrally placed magnesium

TABLE I
Density, Average Weighted Mean Graylevel, and Average Atomic Number Data of the Simulated Tissues Used in This Study

Material	Density (g/cm^3)	Average WMGL Mean (±SD)	Average Atomic Number
Simulated bone tissues			
32% HA/68% Epoxy[a]	1.59	52.92 (3.48)	10.15
33.5% HA/66.5% Epoxy	1.66	56.52 (3.37)	10.22
35% HA/65% Epoxy	1.67	68.40 (3.09)	10.47
36.5% HA/63.5% Epoxy	1.69	72.13 (3.06)	10.55
38% HA/62% Epoxy	1.72	75.31 (2.79)	10.61
41% HA/59% Epoxy	1.77	91.46 (2.90)	10.95
42.5% HA/57.5% Epoxy	1.83	87.95 (2.99)	10.87
44% HA/56% Epoxy	1.90	95.56 (3.34)	11.03
45.5% HA/54.5% Epoxy	1.95	93.86 (3.39)	11.00
47% HA/53% Epoxy	1.98	101.01 (3.08)	11.14
48.5% HA/51.5% Epoxy	1.99	106.83 (3.05)	11.26
50% HA/50% Epoxy	2.07	119.31 (3.66)	11.52
Compositional comparisons			
8% Br/33% HA/59% Epoxy	1.73	84.81 (2.88)	9.64
14% Br/27% HA/59% Epoxy	1.69	67.92 (3.15)	8.84
41% HA/59% Epoxy	1.77	91.46 (2.90)	9.95
Pure minerals (Imaged under different conditions)			
Brushite	2.30	33.79 (10.16)	11.85[b]
HA	3.14	138.90 (12.90)	14.06[b]

WMGL = weighted mean graylevel, SD = standard deviation, HA = hydroxyapatite, Br = brushite.
[a]All simulated bone tissues are shown as volume percentages of each constituent.
[b]Average atomic numbers of Br and HA were calculated using the method of Lloyd, 1987 (ref. 26).
Note. The average atomic number increases with the increasing volume of HA with few exceptions. The exceptions were attributed to local mineral content heterogeneities that resulted from the manual mixing technique. Compositional comparisons were made to demonstrate the role of adding the lower-atomic-number constituent brushite (Br) to the mineral component (see also Figs. 3 and 4). Average atomic number of the mixtures were calculated from the least squares linear regression equation of the pure standards.

wire also served as the main calibration standard, as described below.

The specimen containing the pure materials and simulated tissues was manually ground and polished to an optical finish using previously described methods.[12,15] The bottom surface of the specimen was then ground so that the thickness of the corners and the edges were within a tolerance of ± 50 μm. This tolerance served to eliminate graylevel changes that have been reported to occur when variability in the specimen working distance exceeds ± 100-μm.[12] To avoid graylevel variability associated with surface charging during SEM/BSE imaging,[13] the specimen was lightly coated with gold ($Z = 79$) for 75 s at 70 μm Hg and 10 mA (Hummer Model VI-A, Technics, LTD., Alexandria, VA).

The specimen was mounted on a metal base and placed on the stage of a JEOL JSM-T330A scanning

TABLE II
Density, Average Weighted Mean Graylevel, and Average Atomic Number Data of the Pure Calibration Materials Used in This Study

Material	Density (g/cm^3)	Average WMGL Mean (±SD)	Average Atomic Number
Pure Standards and Epoxy			
Magnesium oxide (MgO)	3.58	64.35 (2.39)	10.41
Aluminum oxide (Al_2O_3)	3.97	74.00 (2.45)	10.65
Magnesium	1.74	152.96 (2.69)	12.00
Aluminum	2.69	184.78 (3.38)	13.00
Epoxy	1.11[a]		

Abbreviations as in Table I.
[a]The density of the epoxy was measured as described in the methods.

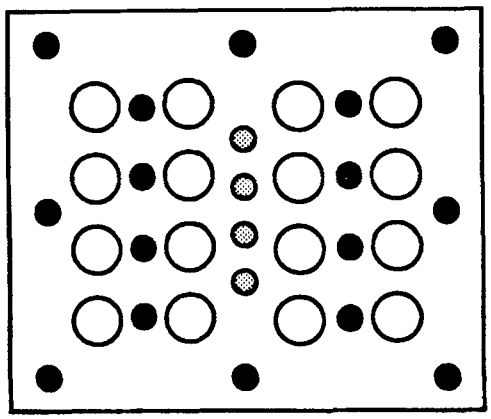

Figure 1. Schematic drawing of specimen containing pure metal standards, minerals, and simulated bone tissues. The dimensions of the specimen are 2.0 × 2.5 cm. ◍, Pure standards used to calibrate the SEM (MgO, Al_2O_3, Mg, and Al); ●, gold-coated magnesium standards used for coating correction; ○, simulated bone tissues and pure minerals.

electron microscope (JEOL USA, Inc., Peabody, MA) with the polished surface placed at a 20-mm working distance and oriented perpendicular (0° tilt) to the incident electron beam. Beam conditions included a 30-kV accelerating voltage and 100-μA load current. The BSE detector consisted of a pair of semiconductor detecting elements (T300-BE152 Backscattered Electron Detector, JEOL Technics LTD., Tokyo, Japan) that were configured between the lower condenser lens aperture and the specimen surface. At the selected 20-mm working distance, the detector was 12 mm from the specimen surface. A voltage regulator (MCR 3000, SOLA, Elk Grove Village, IL) was used to help provide a more uniform power supply to the SEM.

Image analysis system

The system used in this study was a general-purpose hardware-based image analysis system (CRYSTAL, Link Analytical, Redwood City, CA) interfaced directly to the SEM.[15] Graylevel analysis was controlled by an IBM-compatible microcomputer (Zenith Data Systems, Corp., St. Joseph, MI). The monitor of the SEM produced an image with 512 × 570 pixels. At the selected working distance and magnification (×200), the dimensions of one pixel corresponded to approximately 2 μm^2 on the specimen surface. The digitized graylevels span a range from 0–255 in discrete integer values (0 = black, 255 = brightest white). During image capture, the signal to noise ratio was increased by averaging four scans of the electron beam across the specimen surface.

Using a grid system overlaid on the monitor, graylevel analysis was systematically conducted in 10 equal-sized, nonoverlapping regions representing approximately 60% of each captured image. By imaging three fields in each simulated tissue, a total of 30 regions were analyzed, representing approximately 1.1 mm^2 of total surface area analyzed.

According to methods described previously,[12,15] the graylevels in selected regions of BSE images were allocated into 51 graylevel subranges, or bins, and were represented graphically in the form of a graylevel histogram profile (GHP), which is a line graph connecting the maximum numerical values in each graylevel bin. Consequently, a GHP is simply a profile of the frequency distribution of discrete graylevels in the pixels of a selected region in a digitized BSE image. For illustrative purposes, the individual GHPs (n = 30 for each simulated tissue) were summed together into one combined GHP.[12,15]

Imaging sessions

All imaging of the simulated bone tissues was done in one continuous session. The pure brushite and HA pellets were imaged in a separate session because a large adjustment in brightness was required to visualize these relatively higher-atomic-number materials. Calibration of the SEM operating conditions was achieved by superimposing the GHPs of the gold-coated calibration materials.[15] Calibration was checked every third image capture using only the GHP of the gold-coated magnesium standard. It was determined in several pilot imaging sessions that the fluctuation in brightness shifted the placement of the GHP of each pure standard to an equivalent degree (± 1.0%) along the graylevel spectrum. Consequently, the superposition of all standards onto their baseline GHPs was invariably achieved when only one GHP (e.g., that of magnesium) was superimposed onto its baseline GHP. Without exception, all fluctuations in the calibration necessitated only minor alterations in brightness; during SEM operation, adjustment of the contrast and spot size were not required. Calibration procedures were performed if the absolute magnitude of the weighted mean graylevel (WMGL)[15] of the magnesium standard deviated by greater than ± 1.5%. When this occurred, the difference between the WMGLs of the pure magnesium standards captured before and after each set of three images of the simulated bone tissues was subtracted from the initial WMGL. This deviation from the initial WMGL was then added to each of the WMGLs of the simulated bone tissues to correct for filament fatigue or any change in SEM operation conditions.

Average atomic number

Average atomic numbers ($\bar{Z}$) of the minerals and compounds were calculated according to a weight

fraction method described by Lloyd:[26]

$$\bar{Z} = \frac{\sum(NAZ)}{\sum(NA)} \quad (2)$$

where N is the number of atoms of each element with atomic weight A and atomic number Z, and $\sum(NA)$ is the molecular weight. Average atomic numbers of all the simulated tissues were interpolated from the regression equation of graylevel as a function of atomic number for the pure standard materials.

Statistical analysis

To analyze statistically the GHPs obtained in this study, the simulated bone tissue was considered to be the population, the analysis region was considered to be the sample of the population, and the pixels were considered to be "individuals" that comprised the sampled population. The individual GHPs obtained from each analysis region of any given material were assessed for similarity in shape. Skewness,[27] kurtosis,[27] and normality[28] tests were also performed for the individual GHPs. The WMGLs[12] of all the 30 analysis regions obtained for each simulated bone tissue were then averaged and standard deviations determined.

RESULTS

The calibration checks, which were conducted every third image capture, demonstrated that the WMGLs of the magnesium standard deviated from the WMGL of the baseline magnesium standard by -1.1 ± 3.82 graylevels, on average, with a range of -6.7 to $+3.7$ graylevels. This graylevel variability can be attributed to factors associated with the SEM/BSE operating environment, including filament fatigue, electronic drift, and power fluctuations.[5,15] The variabilities in WMGLs of all the magnesium standards (Table II), which were most likely attributable to nonuniformities in coating thickness, were found to deviate from the calibration baseline by -1.2 ± 4.7 graylevels, on average, with a range of -10.1 to $+5.7$ graylevels.

The distributions of the combined GHPs of the pure metal standards are shown in Figure 2. Calibrated BSE images illustrating the graylevel differences of several of the simulated tissues are shown in Figure 3 and their corresponding combined GHPs are shown in Figure 4. Table I lists the averages and standard deviations of the WMGLs of all the individual GHPs. Visual inspection of all the GHPs and the results of the kurtosis, skewness, and normality tests showed that the individual GHPs obtained from any given

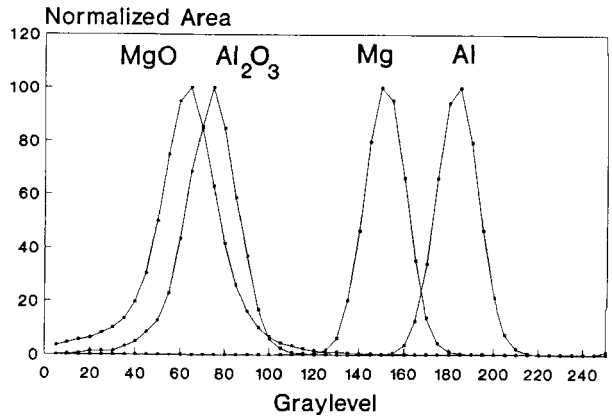

Figure 2. Combined graylevel histogram profiles (GHPs) of the standards that span the atomic number range of the simulated bone tissues. Individual GHPs of each standard were used to calibrate the SEM during the BSE imaging sessions. Atomic numbers of the standards are as follows: magnesium oxide (MgO), $Z = 10.41$; aluminum oxide (Al_2O_3), $Z = 10.65$; magnesium (Mg), $Z = 12$; and aluminum (Al), $Z = 13$.

simulated bone tissue were similarly skewed unimodal bell-shaped curves. The majority (> 65%) of the individual GHPs of the simulated tissues were found to deviate significantly from normality.

Linear regression analysis showed that the atomic numbers of the pure standards were positively correlated to their WMGLs ($r^2 = 0.985$) but had a negative correlation to their densities ($r^2 = 0.499$). The mineral content of the simulated bone showed positive correlation to their average atomic numbers ($r^2 = 0.965$) and density ($r^2 = 0.978$) (Fig. 5). The average WMGLs of the simulated bone tissues also correlated to mineral content ($r^2 = 0.965$) and density ($r^2 = 0.923$) (Fig. 6). Linear regression of data in Table I shows that a 1% increase in mineral content of the simulated bone tissues corresponded to a 0.026 ± 0.001 ($\pm$ standard error) g/cm^3 increase in density, a 3.28 ± 0.20 ($\pm$ standard error) increase in the average WMGL, and a 0.068 ± 0.004 ($\pm$ standard error) increase in average atomic number, when using the SEM operating conditions selected for this study.

Table I lists the graylevel data comparing the 41% simulated tissues containing brushite and HA to the 41% simulated bone tissue containing only HA. Although these simulated tissues had equivalent mineral content, the brushite-containing simulated tissues exhibited darker graylevels and lower densities than the HA simulated bone tissue, which is a result that can be attributed to brushite's lower average atomic number and lower density, respectively (Fig. 3 and Table I). The WMGLs of the pure brushite and HA pellets also exhibited differences consistent with those shown by their average atomic numbers (Table I). The relatively larger standard deviations of these pure

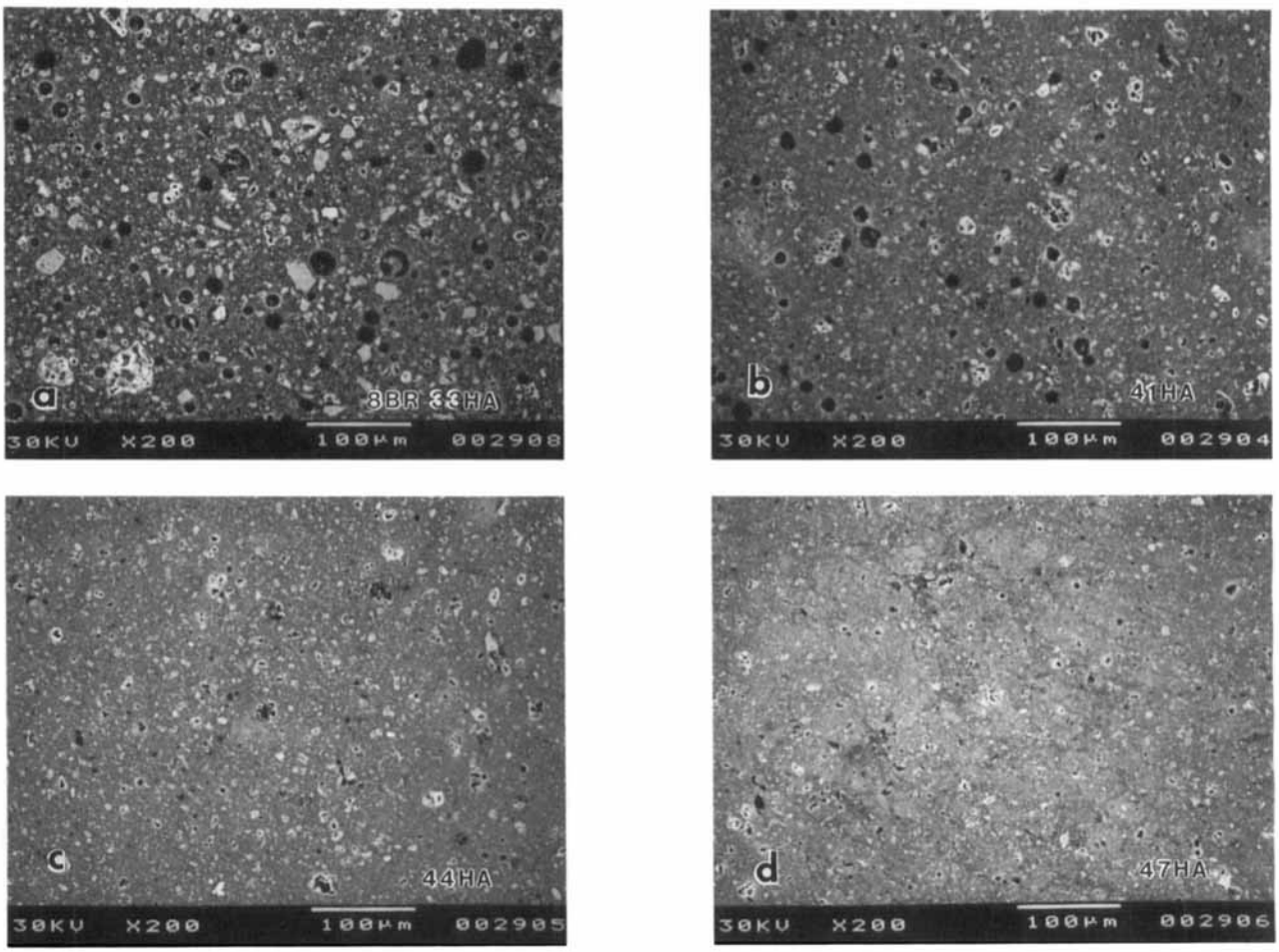

Figure 3. BSE images showing graylevel differences between four of the simulated tissues. Progressively whiter graylevels are seen as the mineral content is increased from 8% brushite/33% HA (a), to 41% HA (b), 44% HA (c), and then to 47% HA (d). Note that the graylevel in the BSE image of the 8% brushite/33% HA (41% mineral content) simulated bone tissue (a) is lower than the 41% HA simulated bone tissue (b). This difference can primarily be attributed to the lower average atomic number of the brushite (Br) phase.

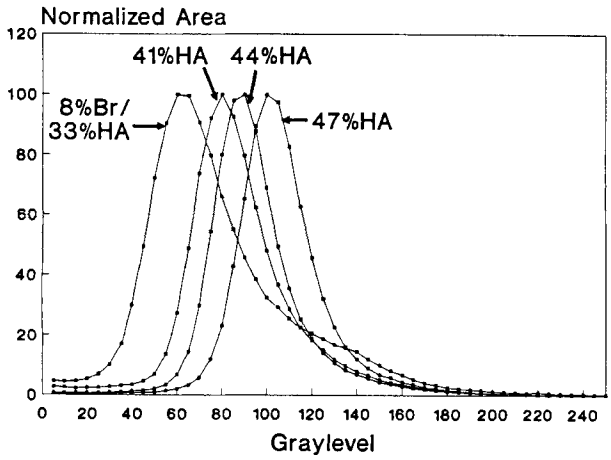

Figure 4. Combined graylevel histogram profiles corresponding to the BSE images seen in Figure 3. Again, note the progression of the graylevel histogram profiles along the abscissa with the exception of the simulated bone tissue containing the lower atomic number brushite (Br).

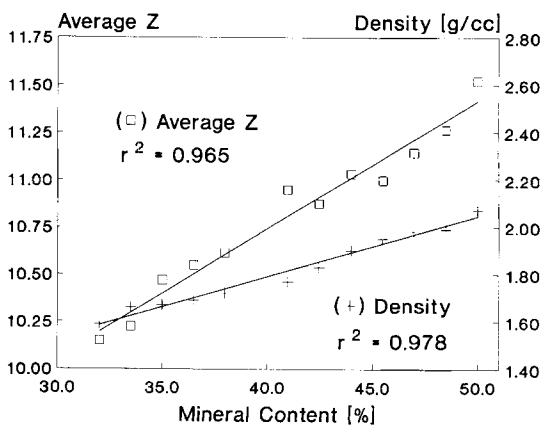

Figure 5. Best-fit regressions demonstrating highly linear relationships and positive correlations between mineral contents and both average atomic numbers (□) and densities (+) of the HA-containing simulated bone tissues.

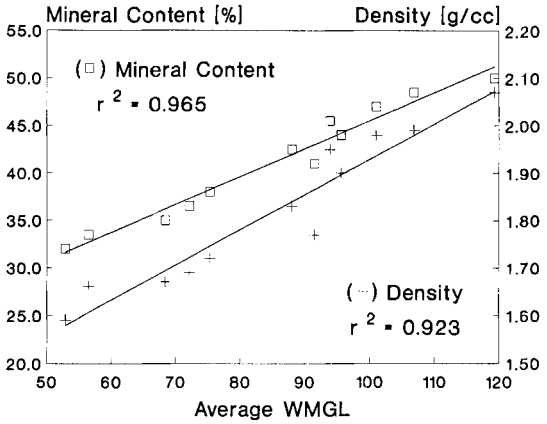

Figure 6. Best-fit regressions demonstrating highly linear relationships and positive correlations of weighted mean graylevels from the HA simulated bone tissues to both mineral content (□) and density (+) (See Fig. 4 and Table I).

minerals can be attributed to topographic irregularity that was observed on the surface of these pellets.

DISCUSSION

The present investigation supports the hypothesis that the graylevel changes in the BSE images of simulated bone tissues are dependent primarily on changes in average atomic number. These changes were shown to be a function of mineral content. The data also demonstrated that when the composition of the mineral component is held constant, using only HA for the simulated tissues, the graylevel changes can also be related to density. The atomic-number-dependent graylevels seen in BSE images of the simulated bone tissues are consistent with basic principles of atomic-number-contast BSE imaging described by Robinson and coworkers.[13,14] Using pure and composite materials, they showed that the voltage output of the BSE detector is dependent on atomic number and that the proportion of electrons backscattered from these materials parallels BSE detector voltage outputs through a broad range of atomic numbers. They also concluded that, after controlling for image contrast changes due to topography, charging, and cyrstallographic orientation, the voltage output of the BSE detector is dependent upon the atomic number of the imaged material [Fig. 7(A)]. Since graylevels in digitized BSE images are proportional to the corresponding voltage outputs of the BSE detector, the graylevel of any pixel has a fundamental and direct relationship to the average atomic number of the corresponding location in the target material.[2,12,15] Through the use of automated image analysis equipment,[12] these fundamental relationships allow the average atomic number to be determined for discrete regions of bone. Image analysis allows the BSE graylevels of the bone image to be quantified, and these graylevel values may then be related to atomic number by comparison with the graylevels of pure standard materials.

The graylevels seen in BSE images of actual bone tissue (Fig. 8) resemble the shades of gray observed in conventional microradiographs of actual bone tissue, where darker graylevels represent tissue of relatively lower density and whiter graylevels represent tissue with higher density.[5,29,30] After observing these similarities, Reid and Boyde[5] hypothesized that digitized BSE images could be used to assess microscopic differences in tissue mineralization. However, the meaning of the graylevels in BSE images of bone tissue remained confused by terminology[1–11] that conflicted with the basic principles of backscattered electron interactions and atomic-number-contrast BSE imaging technology. The results of the present investigation demonstrate that graylevel variations in simulated bone tissue may be correlated to density, provided that the composition of the mineral component is held constant. Since changes in the composition of the mineral component are generally negligible,[25,31] the suggestions of Reid and Boyde relating BSE graylevel to

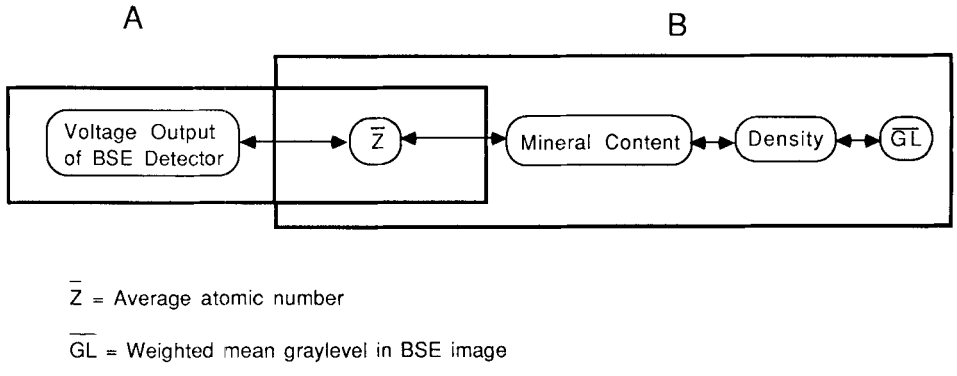

Figure 7. (A) Diagram of correlations previously established between atomic numbers of pure elements and compounds and their corresponding voltage outputs of the BSE detector (ref. 13). (B) Diagram of the correlations that were experimentally established in this study between mineral contents, densities (g/cm^3), atomic numbers, and weighted mean graylevels of the simulated bone tissues.

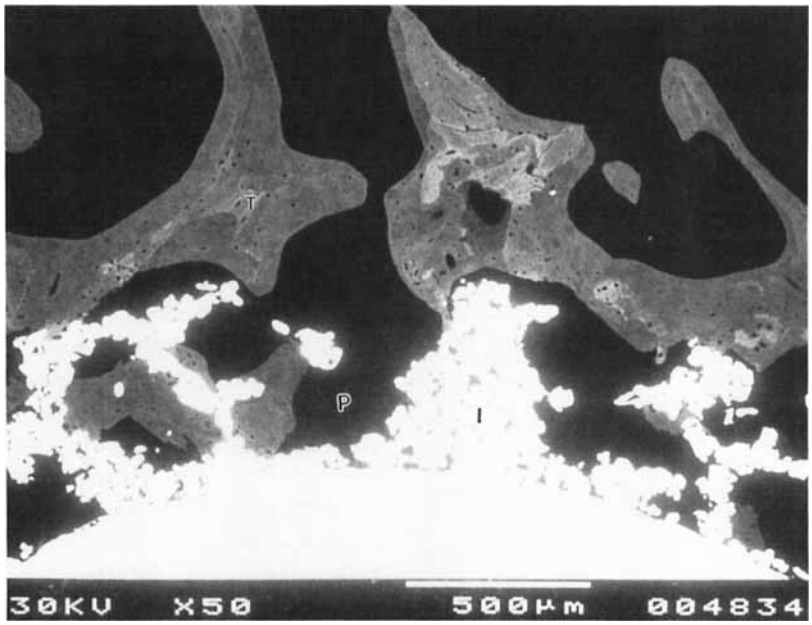

Fig. 8. Backscattered electron image of bone tissue (T) ($\overline{Z} \approx$ between 10 and 12) embedded in a block of polymethyl methacrylate (P) ($\overline{Z} \approx 6.5$) showing ingrowth of bone into the porous coating of a composite metal implant (I) comprised primarily of titanium ($\overline{Z} \approx 22$). Multiple shades of gray, or graylevels, seen in the bone tissue are considered to be related to differences in average atomic number, mineral content and density (g/cm^3).

density are essentially supported. However, the negative correlation between the WMGLs and densities of the pure metal standards, and the fact that the densities of pure elements do not exhibit a smooth monotonic relationship with density or electron backscatter fraction,[12] demonstrated that Reid and Boyde were mistaken in stating, "The backscattering of electrons is a process which is dependent on the atomic number of an element and hence is also proportional to density."[5] Bloebaum et al.[12] have illustrated the fallacy in this statement by showing a darker BSE image graylevel for pure beryllium ($Z = 4$, $\rho = 1.85$ g/cm^3) when compared to pure magnesium ($Z = 12$, $\rho = 1.74$ g/cm^3). The present study demonstrated that the correlation between density and graylevel results are due to the coincidence of the close relationship between density and mineral content (when the mineral composition is held constant), and the association of both of these factors with atomic number [Fig. 7(B)].

The term "mineral content" (Eq. [1]), as used in the present study to describe graylevel variations in atomic-number-contrast BSE images, is consistent with mineralization that occurs during normal maturation and aging of bone tissue. During the process of mineralization, mineral occupies an increasingly larger fraction of the volume of the bone tissue, resulting in an increase in the mineral content of the bone tissue.[17,18] Mineralization is the process that is primarily responsible for causing growth and age-related increases in the density of bone tissue.[24,32–34] Increases in mineral content are also accompanied by decreases in water content[35] and changes in both relative proportions and compositions of collagenous and noncollagenous constituents.[34,36,37] With maturation and aging, changes also occur in the composition, crystallography, crystal size, and density of the inorganic component of bone tissue.[18,33,37–39] Since many of these changes are inextricably linked and often occur synchronously throughout ontogeny, it is important to determine whether changing proportions and compositions of the main components have any influence on graylevels of BSE bone images.

In actual bone tissue, crystallization of hydroxyapatite has been shown to occur within collagen fibrils,[40] and a large portion of the bone mineral is actually within collagenous tissue fibers at all stages of tissue maturation.[33] Therefore, the process of bone mineralization produces a relatively homogeneous composite of the mineral and organic matrix components. Because of this intimate association between the mineral and organic matrix of bone tissue, the incident electrons impinging into a bone tissue specimen would interact with both of these components. Consequently, the influence of the lower-atomic-number organic matrix ($Z \approx 6.5$) of the bone tissue should receive consideration, in addition to that of the higher-atomic-number inorganic component ($Z \approx 14$), as a constituent that contributes to graylevel variations in BSE images of bone tissue.

It has been speculated that brushite is the calcium-phosphate phase formed at the commencement of, and perhaps during the subsequent early stages of, mineralization.[24,25] Yet, whether brushite even occurs in minor amounts in embryonic bone

tissue is controversial.[38,41] Octacalcium phosphate ($Ca_8H_2[PO_4]_6 \cdot 5H_2O$),[31,42] a whitlockite phase ($Ca_9Mg[HPO_4][PO_4]_6$,[43] and β-tricalcium phosphate ($Ca_3[PO_4]_2$),[31] have been detected as coexisting with an apatite phase in normal and pathologically mineralized bone, dental, and other tissues. Nonetheless, these non-HA calcium-phosphate mineral phases have been shown to be present in an amount that typically represents less than 1.0% of the mineral component by weight.[25,31] It has been suggested that the relatively small quantities of these non-HA mineral phases would be expected to have a negligible effect on the graylevels in BSE images in bone and dental tissues when using the SEM/BSE calibration techniques described in the present study and image analysis systems that are currently available for quantifying atomic number contrast from graylevels in digitized BSE images.[44] However, since nearly 60 distinct biogenic mineral phases have been described in the animal kingdom,[45] mineral composition may be an important consideration when analyzing graylevels in BSE images of mineralized tissues from organisms that may contain non-HA mineral phases.

When interpreting the meaning of graylevels in BSE images of bone tissue, consideration should also be given to the potential influence of impurities in the mineral component. Ions of Na, Mg, K, Cl, and other elements and molecules may become incorporated into the crystal lattice of apatites or may become absorbed onto the surface of mineral crystallites during normal aging and maturation.[31] Carbonate (CO_3^{-2}) is the impurity that is typically present in the highest concentration in bone tissue.[31] Age-related increases in this constituent and in other elements may either directly or indirectly facilitate additional changes in the composition of the bone mineral,[31] which could result in unrecognized changes in the average atomic number of the bone tissue.[44] In addition, consideration should also be given to the graylevel variations caused by alterations in the stoichiometry of the bone mineral component that may result from certain drug therapies, such as the use of fluoride for the treatment of osteoporosis.[46,47] Careful scrutiny of the bone mineral composition data reviewed by LeGeros[31] shows that these impurities typically occur in relatively small amounts, supporting suggestions that these compositional changes would produce minor ($< 5.0\%$) to negligible ($< 1.0\%$) changes in WMGLs.[44] Correlated mineral composition analyses are in order whenever the compositional differences might be of sufficient magnitude to influence graylevels in BSE images that are used for discerning relative differences in the mineral content of bone or other mineralized tissues.

The objective of this investigation was to test the hypothesis that graylevels in BSE images of simulated bone tissues can be interpreted and understood in the context of normal mineralization and fundamental principles of atomic-number-contrast BSE imaging. This objective was accomplished by demonstrating that changes in mineral content of simulated bone tissues are positively correlated to changes in density, average atomic number, and WMGL in the BSE image. In view of these results, graylevels in BSE images of bone tissue can now be understood and interpreted using nomenclature that describes the process of mineralization in bone tissue and is consistent with fundamental concepts of atomic-number-contrast BSE imaging.

The authors acknowledge the support of the Department of Veterans Affairs Medical Center, Salt Lake City, UT, and the Whitaker Foundation. We thank Dr. Brent Constantz of Norian Corporation for his helpful suggestions and for providing some of the materials used in this study, Mark T. Nielsen for his helpful suggestions, Lois Mayton for her technical assistance, and Gwenevere Shaw for her assistance in manuscript preparation.

References

1. A. Boyde and S. Jones, "Backscattered electron imaging of dental tissues," *Anat. Embryol. (Berl.)*, **168**, 211–226 (1983).
2. A. Boyde, "Methodology of calcified tissue specimen preparation for scanning electron microscopy," in *Methods of calcified tissue preparation*, G. R. Dickson (Ed.), Elsevier, Amsterdam, 1984, pp. 251–307.
3. S. A. Reid, "A study of human skeletal maturation using the scanning electron microscope," Ph.D. Thesis, University College of London, 1986.
4. S. A. Reid, "Effect of mineral content of human bone on in vitro resorption," *Anat. Embryol. (Berl.)*, **174**, 225–234 (1986).
5. S. A. Reid and A. Boyde, "Changes in the mineral density distribution in human bone with age: Image analysis using backscattered electrons in the SEM," *J. Bone Miner. Res.*, **2**, 13–22 (1987).
6. A. Boyde and S. Jones, "Backscattered electron imaging of skeletal tissues," *Metab. Bone Dis. Rel. Res.*, **5**, 145–150 (1983).
7. A. Boyde, S. A. Reid, and P. G. T. Howell, "Quantimet/SEM stereology of bone using cathodoluminescence and back scattered electron signals," presented at the Proc RMS, 1983.
8. A. Boyde, E. Maconnachie, S. A. Reid, G. Delling, and G. R. Mundy, "Scanning electron microscopy in bone pathology: Review of methods, potential and applications," *Scanning Electr. Microsc.*, **4**, 1537–1554 (1986).
9. A. Boyde, "Intermethod variation in bone histomorphometry: Comparison between manual and computerized methods applied to iliac bone biopsies," *Bone*, **7**, 235 (1986).
10. S. J. Jones and A. Boyde, "Scanning microscopic observations on dental caries," *Scan. Microsc.*, **1**, 1991–2002 (1987).
11. D. B. Burr, M. B. Schaffler, and R. G. Frederickson, "Composition of the cement line and its possible mechanical role as a local interface in human compact bone," *J. Biomech.*, **21**, 939–945 (1988).

12. R.D. Bloebaum, K.N. Bachus, and T.M. Boyce, "Backscattered electron imaging: The role in calcified tissue and implant analysis," *J. Biomater. Appl.*, **5,** 56–85 (1990).
13. V.N.E. Robinson, N.G. Cutmore, and R.G. Burdon, "Quantitative composition analysis using the backscattered electron signal in a scanning electron microscope," *Scan. Electr. Microsc.*, **11,** 483–492 (1984).
14. *V.N.E. Robinson,* "Materials characterization using the backscattered electron signal in scanning electron microscopy," *Scan. Microsc.*, **1,** 107–117 (1987).
15. T.M. Boyce, R.D. Bloebaum, K.N. Bachus, and J.G. Skedros, "Reproducible method for calibrating the backscattered electron signal for quantitative assessment of mineral content in bone," *Scan. Microsc.*, **4,** 591–603 (1990).
16. L.J. Richelle, "Contribution a l'etude du metabolisme mineral de l'os chez le rat," Ph.D. Dissertation, University de Liege, Liege, 1967.
17. L.J. Richelle, and C. Onkelinx, "Recent advances in the physical biology of bone and other hard tissues," in *Mineral metabolism: An advanced treatise,* C. Comar and F. Bronner, (eds.), Academic Press, New York, 1969, pp. 123–190.
18. L.C. Bonar, A.H. Roufosse, W.K. Sabine, M.D. Grynpas, and M.J. Glimcher, "X-ray diffraction studies of the crystallinity of bone mineral in newly synthesized and density fractionated bone," *Calcif. Tiss. Int.*, **35,** 202–209 (1983).
19. M.B. Schaffler and D.B. Burr, "Stiffness of compact bone: Effects of porosity and density," *J. Biomech.*, **21,** 13–16 (1988).
20. S. Lees and C.L. Davidson, "The role of collagen in the elastic properties of calcified tissues," *J. Biomech.*, **10,** 473–486 (1977).
21. D.B. Carter and W.D. Hayes, "The compressive behavior of bone as a two-phase porous structure," *J. Bone Jt. Surg.*, **59A,** 954–962 (1977).
22. R.A. Robinson, "Physicochemical structure of bone," *Clin. Orthop.*, **112,** 263–315 (1975).
23. E. Pellegrino and R. Biltz, "Mineralization in the chick embryo," *Calcif. Tissue Res.*, **10,** 128–135 (1972).
24. A. Roufosse, W. Landis, W. Sabine, and M. Glimcher, "Identification of brushite in newly deposited bone mineral from embryonic chicks," *J. Ultrastruct. Res.*, **68,** 235–255 (1979).
25. D. Lee, W. Landis, and M. Glimcher, "The solid, calcium-phosphate mineral phases in embryonic chick bone characterized by high-voltage electron diffraction," *J. Bone Miner. Res.*, **1,** 425–432 (1986).
26. G.E. Lloyd, "Atomic number and crystallographic contrast images with the SEM: a review of backscattered electron techniques," *Mineralog. Mag.*, **51,** 3–19 (1987).
27. R.R. Sokal and F.J. Rohlf, *Biometry. The principles and practice of statistics in biological research,* W.H. Freeman & Co., New York, 1981.
28. J. Martinez and B. Iglewicz, "A test for departure from normality based on a biweight estimator of scale," *Biometrika,* **68,** 331–333 (1981).
29. R. Amprino and A. Engstrom, "Studies on x-ray absorption and diffraction of bone tissue," *Acta Anat.*, **15,** 1–22 (1952).
30. J. Jowsey, P.J. Kelly, B.L. Riggs, A.J. Bianco, D.A. Scholz, and J. Gershon-Cohen, "Quantitative microradiographic studies of normal and osteoporotic bone," *J. Bone Jt. Surg.*, **47A,** 785–806 (1965).
31. R.Z. LeGeros, "Apatites in biological systems," *Prog. Crystal Growth Charact.*, **4,** 1–45 (1981).
32. R.M. Biltz and E.D. Pellegrino, "The chemical anatomy of bone," *J. Bone Jt. Surg.*, **51A,** 456–466 (1969).
33. M.J. Glimcher, "The nature of the mineral component of bone and the mechanism of calcification," *Instr. Course Lect.*, **36,** 49–69 (1987).
34. J.B. Lian, A.H. Roufosse, B. Reit, and M.J. Glimcher, "Concentrations of osteocalcin and phosphoprotein as a function of mineral content and age in cortical bone," *Calcif. Tissue Int.*, **34,** S82–S87 (1982).
35. K. Mueller, A. Trias, and R. Ray, "Bone density and composition: Age-related and pathological changes in water and mineral content," *J. Bone Jt. Surg.*, **48A,** 140–148 (1966).
36. C. Lapiere and B. Nusgens, "Maturation related changes of the protein matrix of bone," in *Chemistry and molecular biology of the intercellular matrix,* E. Balazs (ed.), Academic Press, New York, 1970, pp. 55–79.
37. J.M. Burnell, E.J. Teubner, and A.G. Miller, "Normal maturational changes in bone matrix, mineral, and crystal size in the rat," *Calcif. Tissue Int.*, **31,** 13–19 (1980).
38. R. Legros, N. Balmain, and G. Bonel, "Age-related changes in mineral of rat and bovine cortical bone," *Calcif. Tisue Int.*, **41,** 137–144 (1987).
39. S. Chatterji, J. Wall, and J. Jeffery, "Age-related changes in the orientation and particle size of the mineral phase in human femoral cortical bone," *Calcif. Tissue Int.*, **33,** 567–574 (1981).
40. S. Weiner and W. Traub, "Organization of hydroxyapatite crystals within collagen fibrils," *FEBS Lett. 4049,* **206,** 262–266 (1986).
41. C. Rey, M. Shimizu, B. Collins, and M.J. Glimcher, "Resolution-enhanced fourier transform infrared spectroscopy study of the environment of phosphate ions in the early deposits of solid phase of calcium-phosphate in bone and enamel, and their evolution with age. I: Investigations in the v4 PO4 domain," *Calcif. Tissue Int.*, **46,** 384–394 (1990).
42. W. Brown, M. Matthew, and M. Tung, "Crystal chemistry of octacalcium phosphate," *Prog. Crystal Growth Charact.*, **4,** 59–87 (1981).
43. F. Driessens and R. Verbeeck, "The dynamics of bone mineral in some vertebrates," *Z. Naturforsch.*, **41,** 468–471 (1986).
44. J.G. Skedros, R.D. Bloebaum, K.N. Bachus, T.M. Boyce, and B. Constantz, "Influence of mineral content and composition on graylevels in backscattered electron images of bone," *J. Biomed. Mater. Res.*, **27,** 57–64 (1993).
45. H. Lowenstam and S. Weiner, *On biomineralization,* Oxford University Press, New York, 1989.
46. C.Y.C. Pak, "Fluoride and osteoporosis," *Proc. Soc. Exp. Biol. Med.*, **191,** 278–286 (1989).
47. L. Mosekilde, J. Kragstrup, and A. Richards, "Compressive strength, ash weight, and volume of vertebral trabecular bone in experimental fluorosis in pigs," *Calcif. Tissue Int.*, **40,** 318–322 (1987).

Received December 9, 1991
Accepted May 18, 1992